Retraction

Retracted: CT and MRI Imaging Characteristics of Gastrointestinal and Mesangial Reactive Nodular Fibrous Pseudotumor Based on Virtual Reality

Journal of Sensors

This article has been retracted by Hindawi following an investigation undertaken by the publisher [1]. This investigation has uncovered evidence of one or more of the following indicators of systematic manipulation of the publication process:

(1) Discrepancies in scope
(2) Discrepancies in the description of the research reported
(3) Discrepancies between the availability of data and the research described
(4) Inappropriate citations
(5) Incoherent, meaningless and/or irrelevant content included in the article
(6) Peer-review manipulation

The presence of these indicators undermines our confidence in the integrity of the article's content and we cannot, therefore, vouch for its reliability. Please note that this notice is intended solely to alert readers that the content of this article is unreliable. We have not investigated whether authors were aware of or involved in the systematic manipulation of the publication process.

In addition, our investigation has also shown that one or more of the following human-subject reporting requirements has not been met in this article: ethical approval by an Institutional Review Board (IRB) committee or equivalent, patient/participant consent to participate, and/or agreement to publish patient/participant details (where relevant).

Wiley and Hindawi regrets that the usual quality checks did not identify these issues before publication and have since put additional measures in place to safeguard research integrity.

We wish to credit our own Research Integrity and Research Publishing teams and anonymous and named external researchers and research integrity experts for contributing to this investigation.

The corresponding author, as the representative of all authors, has been given the opportunity to register their agreement or disagreement to this retraction. We have kept a record of any response received.

References

[1] S. Li, X. Guo, Y. Liu, and M. Jiang, "CT and MRI Imaging Characteristics of Gastrointestinal and Mesangial Reactive Nodular Fibrous Pseudotumor Based on Virtual Reality," *Journal of Sensors*, vol. 2021, Article ID 7054434, 9 pages, 2021.

Research Article

CT and MRI Imaging Characteristics of Gastrointestinal and Mesangial Reactive Nodular Fibrous Pseudotumor Based on Virtual Reality

Shouhong Li,[1] Xiaohua Guo,[2] Yongjiu Liu,[1] and Moxuan Jiang [1]

[1]*Radiology Department, Jingmen No.1 People's Hospital, Jingmen, 448000 Hubei, China*
[2]*General Surgery Department, Yingde People's Hospital, Jingmen, 448000 Hubei, China*

Correspondence should be addressed to Moxuan Jiang; 09124020@cumt.edu.cn

In recent years, with the continued development and development of science and technology and the increasing maturity of medical technology, reactive nodular fibrous pseudotumors remain difficult to diagnose. Therefore, this paper studies CT and MRI imaging properties based on hypothetical gastrointestinal and mesangial reactive erythema nodosum fibrous pseudotumors to improve the diagnosis and treatment of reactive nodular fibrous pseudotumors. In this study, 48 patients with gastrointestinal and intermediate-reactive erythema nodosum fibrous pseudotumors in the gastrointestinal tract and experimental group were screened and identified by surgical pathology and immunohistochemistry. CT or magnetic resonance imaging was used in all patients. An analysis is performed, and the diagnostic values are compared with the pathological results. Experiments have proved that the postoperative reexamination of reactive nodular fibrous pseudotumors found that single masses are common, tumor sizes are different, and most small nodules have relatively more uniform lesion density, and the density of the plain scan is close to the muscle density, and the delay can be seen after enhancement. When the mass is large, the density is uniform, and low-density foci of different degrees can be seen in some masses, and this part rarely shows enhancement. The imaging phenomenon and clinical features of reactive nodular fibrous pseudotumors have specific features that distinguish them from invasive tumors such as gastrointestinal stromal tumors and provide an important basis for accurate clinical diagnosis and treatment.

1. Introduction

Reactive nodular fibrous pseudotumor is a rare benign tumor-like lesion that occurs primarily in adult males and is primarily associated with abdominal surgery history, local foreign bodies, and gastrointestinal inflammatory lesions. The advantage of MRI scans is that they can provide more signal characteristics to facilitate the diagnosis of tumors. The pathological feature of reactive nodular fibrous pseudotumors is well-defined spindle cells and fibrous tissue is nodular hyperplasia. The fibrous tissue scattered therein appears as cotton-like or linear low-intensity shadows, and diffuse sequence lesions are almost equal or low intensity. After

strengthening, most lesions were not strengthened, and the fibrous tissue corresponding to the inside was delayed. Some tumors show higher levels of enhancement, which may be associated with infiltration of lymphocytes and plasma cells in some areas of the tumor. Therefore, further studies are needed on the characteristics of CT and MRI imaging of reactive nodular fibrous pseudotumors.

Overseas, the diagnosis of reactive nodular fibrous pseudotumor using CT or magnetic resonance imaging technology is much faster than in China, and the development and renewal of reactive nodular fibrous pseudotumor technology is faster. Diagnostic methods for reactive nodular fibrous pseudotumors have been significantly improved and

developed. It is believed that the treatment of CT or magnetic resonance imaging technology will become an important breakthrough in the near future. Turbiville and Zhang believe that reactive nodular fibrous pseudotumor is a relatively rare proliferative lesion, and its clinical symptoms are very similar to cancers of the gastrointestinal tract. There is no special symptom, and it is very easy to cause misdiagnosis [1]. Ohana et al. proposed that CT or magnetic resonance imaging technology can reduce the chance of misdiagnosis when diagnosing reactive nodular fibrous pseudotumor, so that more patients can diagnose reactive nodular fibrous pseudotumor as soon as possible and accurately [2]. Yu et al. make all patients undergo MRI microcoil examinations and use MRI scanners to perform qualitative and quantitative analyses of the lesions, including the number, size and morphological characteristics of the tumors, and the signal-to-noise ratio of the two coil imaging. The diagnosis of gastrointestinal tissue lesions provides a basis [3].

The detection and diagnosis technology of reactive nodular fibrous pseudotumor using advanced CT or magnetic resonance imaging technology has begun in Western countries. Compared to Western countries, the detection and diagnosis technology of reactive nodular fibrous pseudotumor in our country has begun clinically late, and its development is relatively slow. With the continuous progress and development of modern science and technology and the increasing maturity of medical technology, the use of advanced CT or magnetic resonance imaging technology will be an important research work to improve the diagnosis of reactive nodular fibrous pseudotumor. In order to accurately diagnose reactive nodular fibrous pseudotumor, Dissanayake et al. continued to analyze the clinical data of 30 patients with gastrointestinal and mesangial reactive nodular fibrous pseudotumor and analyzed their CT and magnetic resonance imaging images [4]. Sumudu et al. believe that enhancing patients' positive attitude towards treatment can reduce anxiety, depression, and other negative emotions, so as to provide clinical reference for prolonging the survival time of cancer patients, improving the quality of life of patients and promoting the recovery of the disease [4]. Shields and Shields successfully use compression detection technology for cardiac dynamic imaging as it transforms the time-varying image by performing a wavelet transform in the spatial domain and then a Fourier transform in the temporal domain along the temporal direction [5].

This article is to deepen the understanding of the gastrointestinal and mesangial reactive nodular fibrous pseudotumor. In the prognosis of abdominal surgery, there are symptoms such as mass hyperplasia, and the gastrointestinal and mesangial reactive nodular fibrous pseudotumor should be considered a possibility to reduce misdiagnosis of reactive nodular fibrous pseudotumor and overtreatment of patients. At the same time, in the diagnosis of reactive nodular fibrous pseudotumor, we will study the imaging characteristics of CT and magnetic resonance imaging and spread this technique to clinical practice so that reactive nodular fibrous pseudotumor can be obtained quickly.

2. Gastrointestinal and Mesangial Reactive Nodular Fibrous Pseudotumor

2.1. Magnetic Resonance Imaging

2.1.1. MRI Physics Algorithm

(1) Spin and Precession. The direction of the magnetic field of the hydrogen nucleus is not consistent with the direction of the external magnetic field, but always has a certain angle with it and rotates around the external magnetic field like a top. This phenomenon is called precession [6]. The frequency of the hydrogen nucleus precession can be derived from the Lamo equation:

$$\omega = \gamma B. \tag{1}$$

In formula (1), ω represents the angular frequency of the atomic nucleus precession, γ represents the magnetorotation ratio, and B represents the field strength of the external magnetic field. For the same kind of particles, the gyromagnetic ratio γ is constant, which is determined by the characteristics of each particle.

(2) Resonance. After receiving the appropriate external source pulse, the net magnetization direction of the nucleus is deflected in the direction of 90°, and the resonance phenomenon can be obtained by Equation (2).

$$\theta = \gamma B_1 \tau. \tag{2}$$

Among them, τ represents the action time of the radiofrequency pulse, B_1 represents the intensity of the radiofrequency pulse, and γ refers to the gyromagnetic ratio.

(3) Relax. Like the flipped net magnetization vector, the relaxation is also divided into two parts on the xy plane and the z axis direction. The M_x component and M_{xy} component can be obtained by formulas (3) and (4), respectively, according to the change of time.

$$M_z(t) = M_0\left(1 - e^{-t/T1}\right), \tag{3}$$

$$M_{xy}(t) = M_0 e^{-t/T2}. \tag{4}$$

It is worth mentioning that the $T1$ and $T2$ times are not the same, and the time $T1$ required for recovery is 5 to 10 times longer than the decay time $T2$. Therefore, although the recovery and attenuation start at the same time after the RF pulse is removed, the two processes are independent of each other [7, 8].

(4) Receive Signal. After the pulse is turned off, the spin hydrogen nuclei release the energy absorbed during the pulse and return to equilibrium. At this time, the receiving coil can immediately detect the oscillation signal and the

attenuation signal. The free induction attenuation is actually the transverse magnetization M_{xy} component the induced current in the receiving coil. This current signal can be expressed as

$$M_{xy(t)} = M_0 e^{-t/T2^*} (\cos \omega_0 t), \tag{5}$$

where $T2^*$ is the decay time of transverse magnetization M_{xy} under the combined action of the external magnetic field and the spin-spin interaction of the hydrogen nucleus. Different from the decay time of $T2$, $T2$ mainly depends on the spin-spin interaction.

2.1.2. Real-Time Online Dynamic Magnetic Resonance Imaging Based on Frame Prediction Technology

(1) Concrete Modeling of Real-Time Online Algorithms. The acquisition model of dynamic magnetic resonance imaging data can be succinctly expressed as follows:

$$y_t = RFx_t + \eta. \tag{6}$$

In Equation (6), x_t represents the image frame at time t; y_t represents the spatial information at time t; F represents the Fourier transform, which converts the signal from the image domain to the spatial domain; R represents the spatial undersampling template; and η represents the noise.

Formulate dynamic magnetic resonance imaging reconstruction as a dynamic system:

$$x_t = x_{t-1} + u_t, \tag{7}$$

$$y_t = RFx_t + \eta_t, \tag{8}$$

where x_t is the state variable, y_t is the observer, η_t is the observed noise, and u_t is the increment between adjacent state variables. In order to reduce the space complexity of the Kalman filter, the covariance matrix of u_t takes a diagonal matrix, which means that the motion/density changes between pixels are irrelevant [9, 10]. The image frame at time t can be expressed as

$$x_t = x_{t-1} + \nabla \tilde{x}_t. \tag{9}$$

∇x_t represents the difference between the current frame and the previous frame. Since the motion/density is gradual and is always limited to a few areas, the residual image ∇x_t will show sparseness. In the following reconstruction, the residual graph can be obtained by solving a l_p norm minimization problem:

$$\min_{\nabla x_t} \|\nabla x_t\|_p^p, \text{ subject to} \|y_t - RF\nabla x_t\|_2^2 \le \varepsilon, \ 0 < p < 1. \tag{10}$$

Here, $\|\bullet\|_p$ and $\|\bullet\|_2$ are the l_p norm and l_2 norm, respectively, and ε is the energy level of noise. This method avoids making unrealistic assumptions like Kalman filtering and does not use too complicated algorithms. Even if it is oper-

ated on an ordinary computer, the reconstruction speed can be close to the real-time standard [11, 12].

(2) MPOD Prediction Method. MPOD uses a simple model to predict the current frame, as shown in Equation (11):

$$\tilde{x}_t = x_{t-1} + \nabla \tilde{x}_t. \tag{11}$$

In the above formula, $\tilde{x}_t$ represents the predicted frame, and $\nabla \tilde{x}_t$ is the estimated amount of motion. So, the problem at this stage is how to estimate $\tilde{x}_t$. Here, the estimation of $\nabla \tilde{x}_t$ is calculated based on the actual amount of motion ∇x_{t-1} between the first three frames [13, 14]. Assume that the amount of motion between consecutive frames conforms to a simple linear dynamic model:

$$\nabla x_{t-1} = \beta \bullet \nabla \tilde{x}_{t-2} + \delta. \tag{12}$$

Radiotherapy is one of the main treatment methods for head and neck squamous cell carcinoma. The fundamental purpose of precise radiotherapy is to increase the dose in the target area, while giving the greatest protection to surrounding tissues and organs. The application of techniques such as cone beam tomography and CT simulation three-dimensional planning can help implement precise positioning during radiotherapy, so as to better take advantage of the highly conformable dose of intensity-modulated radiation therapy. δ is the estimation error that is normally distributed. The amount of motion in the current frame can be estimated according to

$$\nabla \tilde{x}_t = \beta \bullet \nabla x_{t-1}. \tag{13}$$

The valuation of β can be obtained by Tikhonov regularization:

$$\min_{\beta} \|\nabla x_{t-1} - \beta \bullet x_{t-2}\|_2^2 + \lambda \|\beta\|_2^2. \tag{14}$$

Equation (14) can be reexpressed as

$$\min_{\beta} \sum_i \left(\nabla x(i)_{t-1} - \beta(i) \nabla(i)_{t-2} \right)^2 + \lambda \beta(i)^2. \tag{15}$$

Simplification:

$$\beta(i) \left(\nabla(i)_{t-2}^2 + \lambda \right) = \nabla x(i)_{t-2} \nabla x(i)_{t-1}, \tag{16}$$

$$\beta(i) = \frac{\nabla x(i)_{t-2} \nabla x(i)_{t-1}}{\nabla x(i)_{t-2}^2 + \lambda}. \tag{17}$$

Finally, the solution of matrix vector β can be expressed as

$$\phi = y - RF\tilde{x}, \tag{18}$$

$$\beta = \frac{\nabla x_{t-1} \cdot \nabla x_{t-2}}{(\nabla x_{t-1} \cdot \nabla x_{t-2} + \lambda)}. \tag{19}$$

The calculation of β is very fast, and we can calculate the motion amount of the predicted frame through Equation (13). Then, the final prediction frame can be obtained by formula (11) [15, 16].

2.2. Smart Medical

2.2.1. Smart Medical Service Model.
The service model of smart medical cloud service is an innovation of the service model of the traditional medical system. The composition of the traditional hospital system is independent, the systems are independent of each other, there is a lack of integrated data standards, and the interoperability between the systems. Since medical data cannot be shared, a lot of data is accumulated in various systems, but it cannot be mined and utilized effectively [17, 18]. The smart medical cloud service platform uses a cloud computing service model to move scattered medical resources and data to the cloud to build a medical service resource center and data center. This allows you to share medical services between regions and share medical data between systems. After hospitals, scientific research institutes, CDCs, and other medical institutions expose their unique medical service features to the cloud, patients can enjoy medical services anytime and anywhere through the medical cloud service port. These institutions can then use data from other institutions to conduct archaeological surveys and improve their own medical service capabilities. Finally, a smart medical cloud service ecosystem that can continuously evolve and enrich itself is formed [19, 20].

2.2.2. Smart Medical Cloud Service Resource Center.
Smart medical care builds a new medical service model by integrating multiple medical services. The medical service resource center includes a variety of different services. There is no strong correlation between each medical service, and they operate independently. There will be no failure of one service to affect other services; services can communicate with each other, call, and share to serve users, the cloud service resource center faces multiple types of users [21, 22].

2.2.3. Smart Medical Cloud Service Data Center.
In the traditional hospital information system, various patient medical record data, medical image data, medical activity receipts, etc. are stored separately, and the data cannot be shared, and it is not easy to store for a long time. The smart medical cloud service data center is an aggregation of medical data. By storing the above various medical data in the cloud, large-scale data aggregation is realized [20, 23]. This allows for large-scale sharing of medical data between organizations and regions. At the same time, distributed data storage cannot provide full application value. By storing data scattered in various medical institutions in the cloud, it is possible to perform data mining of large-scale medical data and improve data utilization efficiency.

3. Experimental Design of Magnetic Resonance Imaging Characteristics of Reactive Nodular Fibrous Pseudotumor

3.1. Test Subject.
This trial selected 48 patients with gastrointestinal and experimental group mesangial reactive nodular fibrous pseudotumors who were admitted to a hospital from 2018 to 2020 and were confirmed by surgical pathology and immunohistochemistry and had complete imaging data. The patients were divided into two groups with 24 people in each group. The experimental group was treated with psychological intervention combined with traditional treatment methods; the control group was treated with traditional treatment methods. The period of chemotherapy for all patients was about 3 months, with 1 chemotherapy every 14 days, and each chemotherapy ended. CT or magnetic resonance imaging characteristics were used to analyze all patients. And the patients in the control group are comparable in terms of age, gender, tumor stage, and the use of chemotherapy regimens. All patients found small mesenteric nodules after operation for malignant tumors of the abdominal cavity. The clinical laboratory examination results of all patients were normal, and there was no abnormal increase in tumor markers.

Exclusion criteria include patients that only underwent ultrasound examination alone, patients with missing MRI or CT data, and patients without surgical pathology and immunohistochemistry.

3.2. Evaluation Method.
We use questionnaires and in-depth interviews to understand the financial status of patients in the two groups, the perception, acceptance, concern, and psychological state of chemotherapy and identify psychological interventions for patients in the experimental group in a specific way. Intentional psychological intervention methods based on routine basic care have been added to the experimental group. Health education, cognitive-behavioral therapy, group psychotherapy, supportive care, and social support interventions are given before each chemotherapy. Before and after the intervention, the patient's physician, psychiatrist, and responsible nurse surveyed two groups of subjects, each using the self-assessed depression scale, the self-assessed anxiety scale, and the quality of life scale. I participated in. We compared subjects with depression, anxiety, and quality of life and analyzed the effects of psychological interventions on cancer chemotherapy patients. At the same time, a self-developed patient cognitive, acceptance, and concern questionnaire was used to assess the patient's cognitive level. The survey tool used in the survey method is a survey. The questionnaire uses the Likert 5-step scoring method and is scored from 1 to 5. This means that I do not fully agree with this view, disagree with this view, or disagree with it. You disagree and agree with this perspective. The more you fully agree with this perspective, the higher your score and the more you agree with the subject perspective.

3.3. Medical Radio Image.
Two attending physicians and associate chief physicians with 5 and 20 years of experience in abdominal imaging diagnosis jointly read the pictures,

Table 1: Data sheet of evaluation index system for index reliability testing.

	Very clear	Clear	General	Not clear	Chaotic	Alpha
Physiological function	3.72	4.06	4.77	0.33	0.35	0.8362
Body pain	3.76	4.49	4.75	0.56	0.47	0.8152
General health	3.85	4.39	4.06	0.39	0.25	0.8376
Social function	3.92	3.58	4.09	0.34	0.53	0.7428
Emotional intelligence	3.72	3.84	4.63	0.71	0.33	0.7573
Mental health	4.00	3.63	4.72	0.61	0.48	0.7314

reached a consensus, and compared and analyzed the pathological results. The recorded content includes the size, shape, edge, CT density, MRI signal characteristics, enhancement degree and method, and surrounding relationship of the lesion.

3.4. Statistical Processing. SPSS23.0 software was used for data processing, and the count data was expressed in percentage (%), k is the number of data in this experiment, σ^2 is the variance of all survey results, and $P < 0.05$ indicates that the difference is statistically significant. The formula for calculating reliability is shown in Equation (20).

$$a = \frac{k}{k-1}\left(1 - \frac{\sum \sigma_i^2}{\sigma^2}\right). \tag{20}$$

4. Magnetic Resonance Imaging Features of Reactive Nodular Fibrous Pseudotumor

4.1. Evaluation Index System Based on Index Reliability Testing. Here, we perform reliability analysis on all reliability indicators of each object, and the reliability indicators we choose for each object are slightly different. The results are shown in Table 1.

It can be seen from Figure 1 that the data obtained from the patient's physiological function, physical pain, and overall health indicators have a very good effect on this experiment ($\alpha > 0.8$). The patient's social function and emotional intelligence data obtained from various indicators of mental health have an acceptable impact on this experiment ($\alpha > 0.7$), which indicates that the CT and magnetic resonance imaging of gastrointestinal and mesangial reactive nodular fibrous pseudotumors are studied in this article. The six indicators selected for the characteristics of imaging and imaging are reasonable, which provide a basis for subsequent experiments.

4.2. Based on Inspection Data

4.2.1. Comparison of the Cognition and Acceptance of Chemotherapy between the Two Groups of Patients before Each Chemotherapy. Through the methods of questionnaires and in-depth interviews, the two groups of patients were understood about their cognition and acceptance of chemotherapy before each chemotherapy. A self-developed questionnaire of patient cognition, acceptance, and concerns was used to evaluate the patient's cognitive level. The results are shown in Tables 2 and 3.
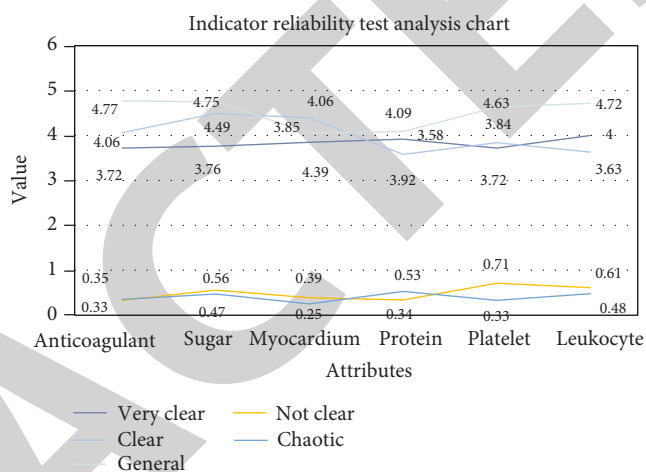

Figure 1: Indicator reliability test analysis chart.

Table 2: Comparison of patients before chemotherapy intervention.

Project	Control group		Test group		X^2	P
	Y	N	Y	N		
Understanding	12	12	14	10	0.056	0.832
Acceptance	10	14	16	8	0.523	0.396
Concern	15	9	15	9	1.991	0.154

Table 3: Comparison of patients after chemotherapy intervention.

Project	Control group		Test group		X^2	P
	Y	N	Y	N		
Understanding	22	2	23	1	15.037	<0.001
Acceptance	6	18	21	3	14.632	<0.001
Concern	20	4	2	22	33.360	<0.001

Tables 2 and 3 show that there is no significant difference between the control and experimental groups regarding concerns about chemotherapy recognition, acceptance, and preintervention chemotherapy side effects ($P > 0.05$). After psychological intervention, there was a significant difference in the perception and acceptance of chemotherapy and concerns about the side effects of chemotherapy compared to the experimental control group ($P < 0.05$). In the later stages of the intervention, there were statistically significant

TABLE 4: Comparison data table of patients' cognition and acceptance of chemotherapy.

Number of chemotherapy	T-understanding	T-acceptance	T-concern	C-understanding	C-acceptance	C-concern
1	2.53	2.84	3.42	2.75	2.51	2.19
2	3.55	3.46	3.24	2.87	2.57	2.46
3	3.33	3.68	2.99	2.68	2.82	3.09
4	4.27	4.39	2.65	3.28	2.99	3.59
5	4.75	4.46	2.35	3.09	3.29	4.17
6	4.73	5.26	1.99	3.21	3.21	4.72

differences in cognitive, receptive, and side effect concerns between the two patient groups ($P < 0.05$).

The changes in cognition, acceptance, and side effect concerns in the two groups of patients during different intervention periods were counted. The results are shown in Table 4.

It can be seen from Figure 2 that the two groups of patients had statistically significant differences in cognitive, acceptance, and side effect concerns during different intervention periods ($P < 0.05$).
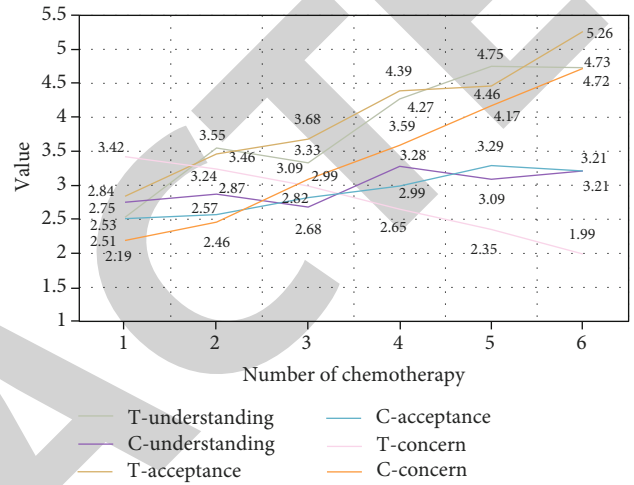
4.2.2. Comparison of Depression and Anxiety between the Two Groups of Patients. We use questionnaires and in-depth interviews to understand the depression, anxiety, and unhealthy mood of the two groups of patients before each chemotherapy. The depression, anxiety, and quality of life of the study subjects were measured with the depression self-rating scale, anxiety self-rating scale, and quality of life scale, a comparative analysis of the effects of psychological intervention for cancer chemotherapy patients; the results are shown in Table 5.

As can be seen from Figure 3, the mood changes in the experimental group after the intervention were better than before the intervention, and the difference was statistically significant ($P < 0.05$), but with depression in the control group after the chemotherapy. Anxiety was significant compared to the two groups of patients; it was better than before the significance of chemotherapy ($P < 0.05$), and the experimental group had postintervention depression compared to the control group and showed a significant improvement in anxiety. There was a significant difference ($P < 0.05$).

4.2.3. Comparison of the Scores of the Two Groups of Patients on the Quality of Life Scale. Through questionnaires and in-depth interviews, we understand the comparison of the quality of life scale scores between the two groups of patients after each chemotherapy. The results are shown in Tables 6 and 7.

It can be seen from Figure 4 that before the intervention, the scores of the experimental group and the control group were not statistically different ($P > 0.05$); during the intervention, the scores of the quality of life dimensions of the experimental group were significantly higher than those of the intervention except for the mental health dimension. Previously, the difference was statistically significant ($P < 0.05$). After the intervention, the test group was significantly better than the control group in all dimensions of the

FIGURE 2: Comparison chart of patients' cognition and acceptance of chemotherapy.

TABLE 5: Comparison data table of patients' depression and anxiety and unhealthy mood status.

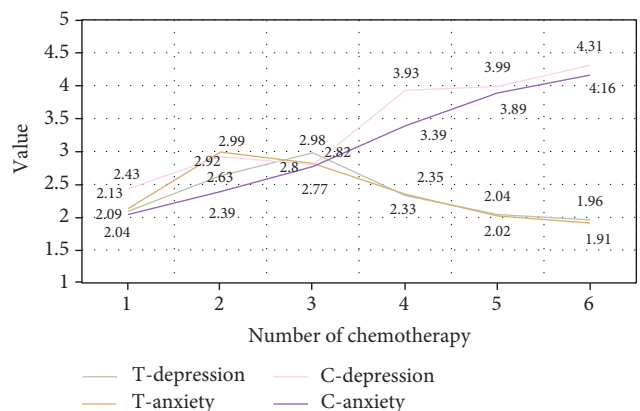| Number of chemotherapy	T-depression	T-anxiety	C-depression	C-anxiety
1	2.09	2.13	2.43	2.04
2	2.63	2.99	2.92	2.39
3	2.98	2.82	2.80	2.77
4	2.33	2.35	3.93	3.39
5	2.04	2.02	3.99	3.89
6	1.96	1.91	4.31	4.16

FIGURE 3: Comparison chart of patients' depression and anxiety.

TABLE 6: Test group quality of life scale score data table.

Number of chemotherapy	Physiological function	Body pain	General health	Social function	Emotional intelligence	Mental health
1	2.39	2.33	2.35	2.94	2.59	2.87
2	2.04	1.80	2.34	2.02	1.99	1.96
3	2.93	2.61	2.89	2.55	2.37	2.96
4	2.77	3.32	3.45	2.71	2.72	2.99
5	3.11	3.41	2.98	2.97	3.01	2.75
6	3.39	3.74	3.29	3.67	3.96	3.60

TABLE 7: Control group quality of life scale score data table.

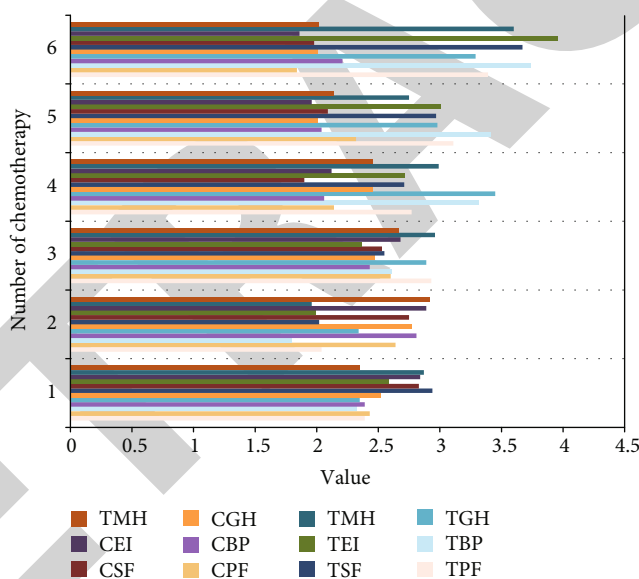| Number of chemotherapy	Physiological function	Body pain	General health	Social function	Emotional intelligence	Mental health
1	2.43	2.39	2.52	2.83	2.84	2.35
2	2.64	2.81	2.77	2.75	2.89	2.92
3	2.60	2.43	2.47	2.53	2.68	2.67
4	2.14	2.06	2.46	1.9	2.12	2.46
5	2.32	2.04	2.01	2.09	1.96	2.14
6	1.84	2.21	2.01	1.98	1.86	2.02

FIGURE 4: Comparison chart of patients' depression and anxiety.

quality of life, and the difference was statistically significant ($P < 0.05$).

4.3. Based on Image

4.3.1. CT Manifestations of Reactive Nodular Fibrous Pseudotumor.
It can be seen from Figure 5 that before treatment, the low-density area of the patient's mass is located at the edge and is irregular, but it can be separated from the solid part. The solid part starts to strengthen from the center, and the arterial phase is slightly strengthened, and the venous phase and the delayed phase are strengthened. The scope gradually increased, and the degree of enhancement gradually increased; after treatment, a slit-like low-density area was seen in the center of the patient's mass, the low-density area was clearly defined, the solid part of the arterial phase was not obvious, and the delayed phase showed continuous and obvious enhancement.

4.3.2. Magnetic Resonance Imaging Analysis of Reactive Nodular Fibrous Pseudotumor.
It can be seen from Figure 6 that the MRI of the patient's reactive nodular fibrous pseudotumor before treatment showed that the tumor had smooth edges, clear borders, and uniform signal; after treatment, the patient's T2WI was mainly high intensity. There are flocculent signal shadows scattered within, and the DWI sequence shows low signal shadows. After enhancement, there is generally no enhancement. There are a few mild enhancement foci scattered within, with clear boundaries. After reexamination of reactive nodular fibrous
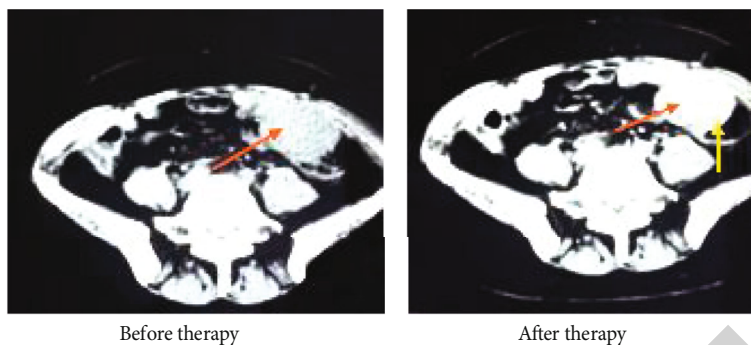
Before therapy   After therapy

Figure 5: Analysis of CT findings of reactive nodular fibrous pseudotumor (from: https://image.baidu.com/).

Before therapy   After therapy
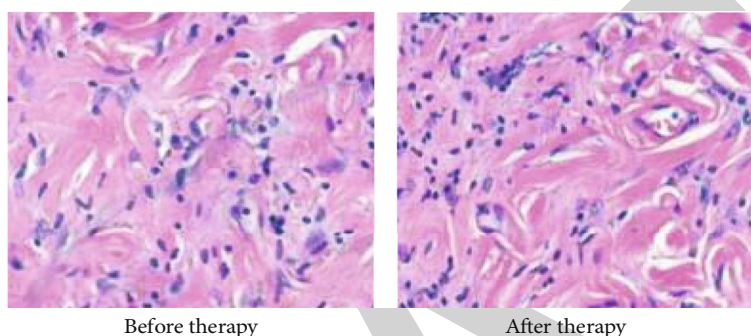
Figure 6: Magnetic resonance imaging appearance of reactive nodular fibrous pseudotumor (from: https://image.baidu.com/).

pseudotumor, it was found that single masses were common, tumor sizes were different, and the density of most small nodules was relatively more uniform, and the density of plain scan was close to muscle density. Delayed enhancement can be seen after enhancement. When it is larger, the density is uniform, and low-density foci of different degrees can be seen in some masses, and this part rarely shows enhancement.

5. Conclusions

Gastrointestinal and mesangial reactive nodular fibrous pseudotumor is an inflammatory fibrous nonneoplastic lesion, which is more common after abdominal surgery or inflammatory irritation. It has an improper prognosis and is prone to recurrence and metastasis. If a mass with delayed uniform enhancement is found after surgical trauma, the boundary is clear, and the T2WI sequence of MRI has characteristic low signal; the possibility of gastrointestinal and mesangial reactive nodular fibrous pseudotumors should be considered to avoid misdiagnosis and overtreatment. Patients' awareness of treatment is generally not high, and some patients may experience cognitive bias during treatment without psychological intervention, leading to aversion to treatment and high concerns about side effects. After effective psychological intervention, you can gradually increase awareness and acceptance of treatment in patients with gastrointestinal malignancies chemotherapy and reduce concerns about side effects. Patients' mood disorders are more obvious than the general public's mood disorders. Psychological interventions can effectively relieve anxiety and

depression in patients, increase treatment compliance, and maintain good mental status during treatment. The drawback of this study is that during the design phase of the study, patients' genders may have different psychological endurance and may have specific effects on the outcome of psychological interventions.

Data Availability

There are no data were used to support this study.

Conflicts of Interest

The authors declare that they have no conflicts of interest.

References

[1] D. Turbiville and X. C. Zhang, "Calcifying fibrous tumor of the gastrointestinal tract: a clinicopathologic review and update," *World Journal of Gastroenterology*, vol. 26, no. 37, pp. 5597–5605, 2020.

[2] M. Ohana, V. Lindner, A. Labani, G. Alemann, H. Lang, and C. Roy, "Fibrous pseudotumor of the tunica vaginalis of the scrotum: is there a typical ultrasound pattern?," *Ultrasound International Open*, vol. 2, no. 1, pp. E34–E36, 2016.

[3] R. Yu, J. Terry, M. Alnassar, and J. Demaria, "Pediatric fibrous pseudotumor of the tunica vaginalis testis," *Asian Journal of Urology*, vol. 3, no. 2, pp. 99–102, 2016.

[4] S. N. Dissanayake, J. Hagen, A. Fedenko, and C. Lee, "Calcifying fibrous pseudotumor of the posterior mediastinum with encapsulation of the thoracic duct," *Annals of Thoracic Surgery*, vol. 102, no. 1, pp. e39–e40, 2016.

[5] J. A. Shields and C. L. Shields, "Tumors and related lesions of the pigmented epithelium," *Asia-Pacific Journal of Ophthalmology*, vol. 6, no. 2, pp. 215–223, 2017.

[6] R. K. Shangareeva, A. A. Mirasov, R. R. Zaynullin, P. Y. Soldatov, and G. R. Valeeva, "Difficulties in diagnosing a foreign body in the gastrointestinal tract (hydrogel) of a 10-month-old child," *Russian Journal of Pediatric Surgery Anesthesia and Intensive Care*, vol. 9, no. 1, pp. 104–109, 2019.

[7] M. Zerrik, H. Echchachoui, Z. Iloughmane et al., "Cannon ball diagnosis and management in a flight attendant candidate," *Aerospace Medicine and Human Performance*, vol. 88, no. 10, pp. 958–961, 2017.

[8] C. W. Chian, Y. S. Lee, Y. J. Lee et al., "Cilostazol ameliorates diabetic nephropathy by inhibiting highglucose- induced apoptosis," *Korean Journal of Physiology and Pharmacology*, vol. 24, no. 5, pp. 403–412, 2020.

[9] H. Lisowska, M. Marciniak, J. Cianciara, and K. Pawełczyk, "A rare case of calcifying fibrous pseudotumor of the pleura with an accompanying vascular anomaly in the pulmonary ligament," *Polish Journal of Cardio-Thoracic Surgery*, vol. 15, no. 1, pp. 59–61, 2018.

[10] K. Xu, L. Guo, H. Bu, and H. Wang, "Daphnetin inhibits high glucose-induced extracellular matrix accumulation, oxidative stress and inflammation in human glomerular mesangial cells," *Journal of Pharmacological Sciences*, vol. 139, no. 2, pp. 91–97, 2019.

[11] R. K. Chaudhary, B. H. Shamsi, and J. P. Xing, "A case with solitary fibrous pseudotumor of the testicular tunica and review of literature," *Transylvanian Review*, vol. 25, no. 22, pp. 5599–5602, 2017.

[12] E. Maheshwari, R. Ram, T. Pandey, G. Bajaj, and K. Jambhekar, "Hepatic inflammatory pseudotumor—a diagnostic challenge: a case report and review of literature," *Journal of Gastrointestinal and Abdominal Radiology*, vol. 2, no. 1, pp. 45–48, 2019.

[13] P. Argyris, P. Anim, and I. G. Koutlas, "Maxillary pseudotumor as initial manifestation of von Willebrand disease, type 2: report of a rare case and literature review," *Oral Surgery Oral Medicine Oral Pathology & Oral Radiology*, vol. 121, no. 2, pp. e27–e31, 2016.

[14] A. R. Roszkowski, A. Witkowska, P. Baranek, A. Rzepakowska, E. Wnuk, and K. Niemczyk, "Rare proliferative and inflammatory pathologies localized in the temporal bone - a review of the literature," *Polski Przegld Otorynolaryngologiczny*, vol. 8, no. 2, pp. 1–5, 2019.

[15] T. A. Potretzke, B. R. Tan, M. B. Doyle, E. M. Brunt, J. P. Heiken, and K. J. Fowler, "Imaging features of biphenotypic primary liver carcinoma (hepatocholangiocarcinoma) and the potential to mimic hepatocellular carcinoma: LI-RADS analysis of CT and MRI features in 61 cases," *American Journal of Roentgenology*, vol. 207, no. 1, pp. 25–31, 2016.

[16] H. Ding, H. Wei, H. Liu, Y. Chen, X. Xue, and H. Weng, "The histopathological features and CT/MRI imaging performances in hepatic angiomyolipoma patients," *Annals of Hepatology*, vol. 16, no. 5, pp. 759–764, 2017.

[17] J. Fang, B. Chen, W. Zhang, H. Song, and L. I. Kui, "CT and MRI features of ovarian fibroma," *Chinese Journal of Medical Imaging Technology*, vol. 33, no. 9, pp. 1366–1369, 2017.

[18] W. U. Hongqing, L. Song, Y. Xiang, X. Zhu, and H. Sui, "CT and MRI features of malignant peripheral nerve sheath tumor of adults," *Chinese Journal of Medical Imaging Technology*, vol. 33, no. 7, pp. 1052–1056, 2017.

[19] C. W. Ding, Q. S. Wang, Q. Y. Guo, J. Zhang, and Z. H. Wang, "CT and MRI features in adult patients with orbital subperiosteal abscess secondary to paranasal sinus mucocele," *Ear, Nose, & Throat Journal*, vol. 96, no. 7, pp. E1–E6, 2017.

[20] E. Bastug, M. Bennis, M. Médard, and M. Debbah, "Toward interconnected virtual reality: opportunities, challenges, and enablers," *IEEE Communications Magazine*, vol. 55, no. 6, pp. 110–117, 2017.

[21] A. S. Rizzo and S. T. Koenig, "Is clinical virtual reality ready for primetime?," *Neuropsychology*, vol. 31, no. 8, pp. 877–899, 2017.

[22] C. T. Chen, S. Y. Chen, C. H. Liao, and S. C. Zeng, "An interactive nanomanipulation visualization based on molecular dynamics simulation and virtual reality," *Transactions-Canadian Society for Mechanical Engineering*, vol. 37, no. 3, pp. 991–1000, 2013.

[23] G. Riva, M. Bacchetta, M. Baruffi, G. Cirillo, and E. Molinari, "Virtual rality environment for body image modification: a multidimensional therapy for the treatment of body image in obesity and related pathologies," *Cyberpsychology & Behavior*, vol. 3, no. 3, pp. 421–431, 2000.